# Optical testing of diamond machined, aspheric mirrors for ground-based, near-IR astronomy

V. John Chambers*[a], Ronald G. Mink[a], Raymond G. Ohl[a], Joseph A. Connelly[a], J. Eric Mentzell[a], Steven M. Arnold[b], Matthew A. Greenhouse[a], Robert S. Winsor[c], John W. MacKenty[c]

[a]NASA/Goddard Space Flight Center, Greenbelt, Md.
[b]Diffraction International Ltd., 11345 Highway 7, #421, Minnetonka, Minn.
[c]Space Telescope Science Institute, 3700 San Martin Drive, Baltimore, Md.

## ABSTRACT

The *Infrared Multi-Object Spectrometer (IRMOS)* is a facility-class instrument for the Kitt Peak National Observatory 4 and 2.1 meter telescopes. *IRMOS* is a near-IR (0.8—2.5 μm) spectrometer and operates at ~80 K. The 6061-T651 aluminum bench and mirrors constitute an athermal design. The instrument produces simultaneous spectra at low- to mid-resolving power ($R = \lambda/\Delta\lambda$ = 300—3000) of ~100 objects in its 2.8×2.0 arcmin field.

We describe ambient and cryogenic optical testing of the *IRMOS* mirrors across a broad range in spatial frequency (figure error, mid-frequency error, and microroughness). The mirrors include three rotationally symmetric, off-axis conic sections, one off-axis biconic, and several flat fold mirrors. The symmetric mirrors include convex and concave prolate and oblate ellipsoids. They range in aperture from 94×86 mm to 286×269 mm and in f-number from 0.9 to 2.4. The biconic mirror is concave and has a 94×76 mm aperture, $R_x$=377 mm, $k_x$=0.0778, $R_y$=407 mm, and $k_y$=0.1265 and is decentered by –2 mm in X and 227 mm in Y. All of the mirrors have an aspect ratio of approximately 6:1. The surface error fabrication tolerances are < 10 nm RMS microroughness, "best effort" for mid-frequency error, and < 63.3 nm RMS figure error.

Ambient temperature (~293 K) testing is performed for each of the three surface error regimes, and figure testing is also performed at ~80 K. Operation of the ADE PhaseShift MicroXAM white light interferometer (micro-roughness) and the Bauer Model 200 profilometer (mid-frequency error) is described. Both the sag and conic values of the aspheric mirrors make these tests challenging. Figure testing is performed using a Zygo GPI interferometer, custom computer generated holograms (CGH), and optomechanical alignment fiducials.

Cryogenic CGH null testing is discussed in detail. We discuss complications such as the change in prescription with temperature and thermal gradients. Correction for the effect of the dewar window is also covered. We discuss the error budget for the optical test and alignment procedure. Data reduction is accomplished using commercial optical design and data analysis software packages. Results from CGH testing at cryogenic temperatures are encouraging thus far.

Keywords: mirrors, asphere, biconic, computer generated hologram, CGH, cryogenic optical testing, *IRMOS*

## 1. INTRODUCTION

The *Infrared Multi-Object Spectrometer (IRMOS)* will see first light in 2003 at the Kitt Peak National Observatory (KPNO) near Tucson, Arizona.[1] Designed as a facility class instrument for the KPNO 4 and 2.1 meter Telescopes, it will explore the micro-electromechanical system (MEMS) spectrometer concept and provide a forefront scientific instrument for a team of scientists led by Dr. John W. MacKenty at the Space Telescope Science Institute (STScI), the NASA/Goddard Space Flight Center (GSFC) and KPNO. *IRMOS* is composed of two all-reflective, imaging systems that are confocal at a MEMS micro-mirror array (MMA; Figure 1).[2] The first stage is designed to relay the telescope focal plane to the MMA. The second stage is the spectrometer, which achieves resolving powers $R = \frac{\lambda}{\Delta\lambda}$ of 300, 1000,

* Correspondence: Email: jchamber@pop500.gsfc.nasa.gov; Telephone: 301-286-9944; Fax: 301-286-0204

and 3000 in the J, H and K bands (0.8--2.5 μm). The use of the MMA and challenging mass and volume constraints lead to a unique design for this spectrometer, requiring the use of off-axis, aspheric mirror prescriptions.[2] Six mirrors are used: two flat fold mirrors, two off-axis, concave conics, one off-axis, convex conic, and one off-axis concave biconic asphere. The fabrication and characterization of these mirrors is challenging.[3]

We briefly discuss the mirror opto-mechanical design, which is covered in more detail elsewhere (Section 2).[3] We describe the measurement of mirror surface error and compare our results to instrument requirements (Sections 3 and 4). Specifically, we cover figure error testing at ~293 K and ~80 K, mid-frequency error measurements (for the flat mirrors), and microroughness measurements. The error budget, data reduction algorithm, and experimental difficulties associated with the cryogenic figure error testing are also discussed (Sections 5 and 6). The impact of the data on system performance is covered by Connelly, et al.[4] We conclude with a summary of our results and the lessons learned from the *IRMOS* mirror test program.

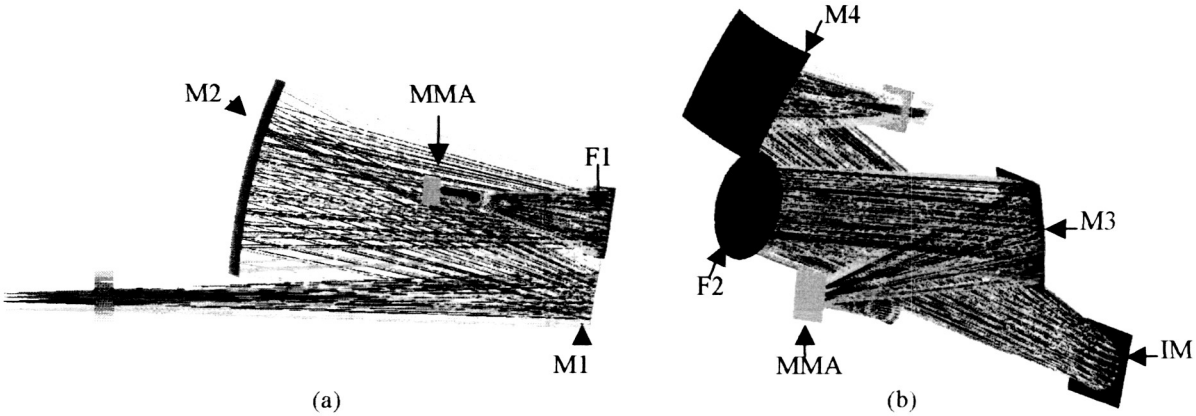


Figure 1. (a) Side view of front-end optics ("stage 1"; focal reducer). (b) Side view of spectrometer optics ("stage 2").

| Mirror | Aperture (mm) X | Y | Radius (mm) (1/c) | Conic | Decenters (mm) X | Y |
|---|---|---|---|---|---|---|
| M1 | 104 | 90 | -694 | 5.8 | 0 | -75 |
| M2 | 284 | 264 | 732 | 0.151 | 0 | -70 |
| M3 | 92 | 77 | 351 | -0.224 | 7 | 135 |
| M4 | 94 | 76 | 377(X) \| 407(Y) | 0.078(X) \| 0.127(Y) | -2 | 227 |
| F1 | 104 | 94 | ∞ | N/A | N/A | N/A |
| F2 | 87 | 87 | ∞ | N/A | N/A | N/A |

Table 1. Mirror prescriptions (293 K).

## 2. OPTICAL AND MECHANICAL DESIGN

A summary of mirror optical and mechanical design is given here. A more detailed description of design and fabrication is presented by Ohl, et al.[3]

### 2.1. Mechanical Design

The use of aluminum 6061 mirror substrates and bench allow for a thermally predictable instrument design. The mirror blanks are stress relieved during fabrication to minimize change in figure error from room temperature to ~80 K.[5] The rear-mounting surface of M2 is depicted in Figure 2. All the mirrors have a ~6:1 aspect ratio and an integral flexure

mounting scheme. The three tabs are designed to flex in order to minimize surface distortion during mounting to the instrument optical bench. We produced at least two mirrors for each element. Characterizing each mirror across all ranges in spatial frequency allows us to designate each mirror as either 'baseline' or 'spare', i.e., one mirror is for instrument integration and the second is a spare. The orientation of the plane of the rear surface of the mirror substrate was chosen such that it is approximately normal to the average normal to the aspheric optical surface in order to make the thickness of the blank approximately constant. The rear surface is thus oriented in a seemingly arbitrary (but known) manner with respect to the vertex. Fabrication and in-process testing is covered by Ohl, et al.[3]

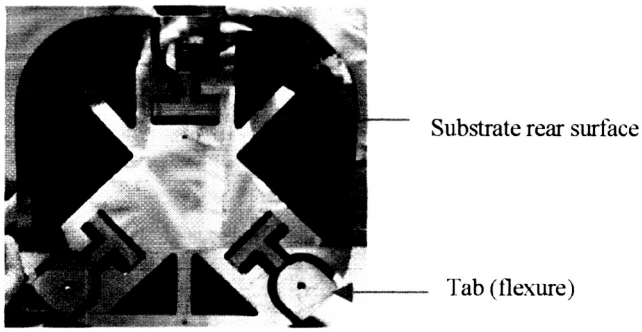


Figure 2. Photo showing rear mounting surface of M2.

### 2.2. Optical Prescriptions and Tolerances

The optical prescription of each mirror is given in Table 1. Note that the radius of M1 specifies it as a convex surface and that M4 is the sole biconic surface. A biconic is a toroid with different X and Y radii and conic constants (i.e., it has no axis of rotational symmetry). The surface error fabrication tolerances for the mirrors are similar. The aperture is located to ± 0.127 mm with respect to the mirror vertex. The rear surface scribe alignment fiducial placement tolerance is ± 0.125 mm and knowledge tolerance is ± 0.025 mm with respect to the vertex. The focus scribe alignment fiducials, one located on all four sides of the substrate, has a best effort placement tolerance and a knowledge tolerance of ± 0.125 mm. The angular orientation of the rear surface is ± 30 arcsec with respect to the vertex. The figure error* requirement for each mirror is < 0.1 λ RMS (λ =632.8 nm) over the full clear aperture, but the sub-aperture specification (for each field angle) is tighter and varies by mirror. The footprint of a single field angle differs for each mirror. The sub-aperture RMS specification is derived from scaling the full aperture specification by the ratio of the sub-aperture to the full aperture areas (Equation 1). Equation 1 results in M2 requiring as low as < λ/19 RMS in a 160 mm diameter while M3 requires < λ/26 RMS in 40 mm diameter (Table 4).

$$x\lambda = (0.1\lambda)\sqrt{\frac{A_{Subap.}}{A_{Fullap.}}} \qquad (1)$$

The full-to-sub-aperture scaling described by Equation 1 assumes that the figure error across the full aperture is a smooth function dominated by low-order terms.[3] The system-level wavefront error budget includes a contribution from each mirror sub-aperture. Our tolerance analysis is based on the conservative assumption that the sub-aperture wavefront has the form of an equal mix of astigmatism and spherical aberration.[6] This model surface is used to calculate the less precise (lower information-content), RMS surface error fabrication specification. In addition, a ~0.05 λ RMS delta is expected for figure error change from room temperature to the operating temperature.[5] If the mirrors do not meet specification, they may cause degraded instrument throughput and/or spectral resolution.

* Surface error with spatial periods > ~10 mm.

The microroughness* requirement for each powered mirror is < 10 nm RMS. The flat mirrors have a goal of < 2 nm RMS microroughness. Tool marks and other small-scale surface features cause scattering. This degrades the throughput of stages one and two and the contrast performance of the stage two spectrometer (spectral purity). These specifications were derived from a rough scatter analysis that assumed that the tool marks on mirrors act like an ideal grating. The flat mirrors were made smoother via "super polishing."[7] The mid-frequency† specification was left open because the vendor was not able to deliver on better than a "best effort" basis.[3] Mirror optical figuring was performed via diamond machining at the Laboratory for Micromachining at the University of Bremen (LFM).‡

## 3. TEST PROCEDURE

### 3.1. Mid-frequency Error and Microroughness

An ADE Phase Shift MicroXAM white light interferometer is used to characterize mirror microroughness.§ The MicroXAM is a non-contact 3D surface profiler capable of spatial resolutions as low as 0.3 nm and an amplitude sensitivity of ~0.01 nm across a 300×410 μm field of view (at ×20 magnification).[8] The MicroXAM's Mapvue™ software uses a fringe-fitting algorithm to calculate a surface error map. For powered mirrors, low order, spherical and cylindrical terms are removed via a least squares fit to the surface error array and entry-wise subtraction.

Aluminum mirrors are soft and susceptible to scratching, so a non-contact method of profilometry is preferred for measuring mid-frequency errors. A Bauer Model 200 Profilometer¶ is used to accomplish these measurements.[9] This laser profilometer has a spatial period range of 10--0.3 mm and an amplitude sensitivity of ~0.05 nm. The raw data is averaged over three, 20 mm scans for the flat mirrors. Sets of scans are taken twice in orthogonal directions across the mirrors, once along the direction of tool marks and once against. Mid-frequency testing of the powered mirrors is omitted for two reasons: the Bauer's testing requirements for aspheric surfaces are complex, and we also found that the mirrors' microroughness interfered with the Bauer's ability to produce mid-frequency measurements.

### 3.2. Null Testing for Figure Error

Null testing requires a test wavefront that matches the component's ideal prescription. Spherical and flat surfaces may be tested with "off the shelf" reference surfaces. The powered *IRMOS* mirrors do not lend themselves to straightforward null tests (Table 1).‖ M1 and M2 are off-axis sections of convex and concave oblate ellipsoids, respectively. These rotationally symmetric oblate ellipsoids could be tested using a traditional null lens with the axis of the test setup aligned with the vertex of the parent surface. However, the off-axis aperture of the part and arbitrary orientation of the rear of the substrate with respect to the vertex introduce additional uncertainty for alignment. One solution would be to test the mirrors while they were still in their single point diamond turning (SPDT) spindle fixtures. However, these fixtures would be too large for cryogenic testing in our dewar. Since M4 is not rotationally symmetric, it is extremely difficult to test the mirror to our specifications with a traditional, rotationally symmetric null lens. Therefore, we used CGHs to null test these mirrors in a straightforward, normal incidence setup at both ~293 and ~80 K.

#### 3.2.1. Figure Testing at Warm

Prior to cold testing, the figures of each of the 12 mirrors (six baseline and six spares) are tested at ambient, room temperature (293 K). The mirrors are each put through at least three warm tests to ensure repeatability from trial to trial. In order to verify best alignment for the figure test setups, we measure the wavefront error as a function of deliberate,

---

* Surface error with spatial periods ≤ ~0.1 mm.

† Surface error with spatial periods > 0.1 mm and ≤ ~10 mm.

‡ Laboratory for Precision Machining, Badgasteiner Str. 2, 28359 Bremen, Germany

§ ADE Phase Shift, 3470 E. Universal Way, Tucson, AZ 85706 USA

¶ Bauer Associates Inc., 177 Worchester Road, Suite 101, Wellesley, MA 02181 USA

‖ Except for M3. A prolate ellipsoid can be tested in double-pass with the focus of the interferometer at one focus and a sphere at the other.[10] We do not present this data here.

measured misalignment. A secondary goal of our testing is to measure as-built alignment fiducial locations with respect to the mirror vertex.

Differences in prescription required a unique CGH setup for each powered mirror. The warm test setup for one of the mirrors is depicted in Figure 3. The M2 test setup (Figure 3a) depicts a Zygo GPI Interferometer emitting a 4 inch converging spherical beam.* The beam passes through a CGH that is magnetically mounted on a six axis mount. The CGH redirects the converging beam in three different manners. It produces a null wavefront in first order that matches the aspheric surface of the M3 mirror. It also produces two beams that converge at the positions of the outrigger fiducials on the backside of the mirror substrate. Another area on the CGH produces a small, collimated beam. The mirrors are mounted using a stress-free mount that affords six degrees of freedom adjustment while allowing theodolite access to the mirror's rear surface and fiducials. A two axis cathetometer and theodolite (via a fold mirror) are positioned behind the mirror mount. Abbreviated test procedures for each mirror are as follows:

1. Flat mirrors
   - Align a reference flat on Zygo GPI interferometer and roughly position the mirror mount in the beam.
   - Center a flat mirror on the mount such that the beam waste overfills the mirror aperture.
   - Rotate the flat in $R_X$ and $R_Y$ until the Zygo beam returns into the interferometer.
   - Further adjust in $R_X$ and $R_Y$ until the reference wavefront is nulled (fringes minimized).
   - Record the surface profile with MetroPro™ software.

2. Mirrors M2, M3, and M4
   - Align a reference sphere on the Interferometer and center the alignment CGH in the converging beam.†
   - Adjust the CGH mount in X, Y, and Z translation until the alignment CGH produces the correct return.
   - Exchange the reference sphere with the reference flat and adjust the CGH mount until the CGH is perpendicular to the collimated beam.
   - Replace the reference sphere and exchange the alignment CGH for the custom CGH null.
   - Roughly position the mirror mount in the null wavefront and measure the position of the collimated CGH beam with the theodolite.
   - Place a view screen on the mount. Measure the positions where the CGH outrigger fiducial beams strike the screen with both the theodolite and the cathetometer.
   - Replace the fiducial view screen with the test mirror and position the mirror's outrigger fiducials to match the position of the CGH fiducial beams.
   - Rotate the mirror in $R_X$ and $R_Y$ until the theodolite's auto-collimated beam verifies that the mirror's back surface matches the position of the CGH's collimated beam.
   - Further adjust the test mirror in rotation ($R_X$ and $R_Y$ ) while compensating in translation (X, Y, and Z) until best alignment is achieved (i.e. lowest system wavefront error).
   - Measure the placement of the mirror's rear, diamond-turned surface as well as the 'as-built' fiducials by recording their new positions at best alignment.
   - Measure the wavefront error as a function of misalignment in order to verify mirror alignment.

3. M1
   - Align the biconvex lens to the collimated LUPI‡ (Laser Unequal Path Interferometer) test leg by overlapping both of the lens surface vertex returns on the LUPI's CCD camera.§ [7]
   - Autocollimate a theodolite off of a reference cube attached to the lens' mount.
   - View the theodolite return from the cube while raising the lens 7 mm to its prescribed position to ensure that the lens does not rotate out of alignment.
   - Align the custom M1 CGH in the spherical, diverging f/4 beam.

---

* Zygo Corporation, Laurel Brook Road, Middlefield, CT 06455 USA

† A reflective alignment CGH is required to transfer spherical test beam alignment (in translations) to the custom CGH null.

‡ Model MIC-1, Buccini Instrument Co., Wilmington, NC.

§ The M1 setup is unique in that it must employ an intermediate biconvex lens in order to null test M1's convex surface.

- Center M1 in the converging null beam and align as per the previous procedure.

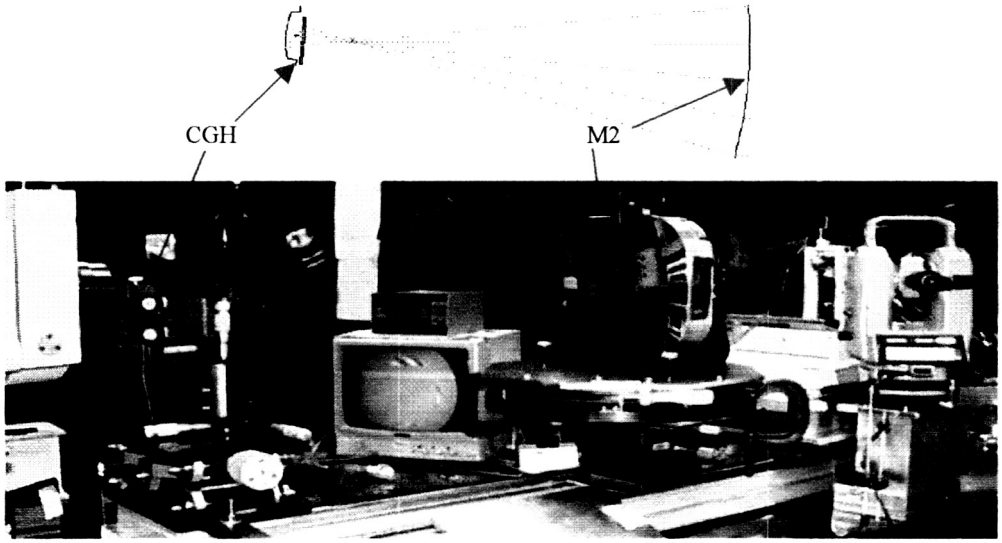


(a)

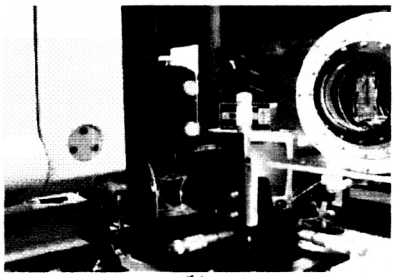

(b)

Figure 3. (a) Figure test setup with ray trace schematic for M2. (b) View of CGH mount and dewar during cold testing.

### 3.2.2. Figure Testing at Cold

Figure 3b depicts cold testing of the M3 mirror. While the process of aligning the CGH matches that of the warm tests, the cryogenic dewar that encloses the mirror prevents alignment using mirror fiducials. The dewar is mounted on a six axis translator with the mirror's surface ~431 mm from the CGH. Inside the dewar, the mirror is simply supported and taped to a diamond turned cold plate that is attached to a cold finger cooled by liquid nitrogen (LN2) flow. The reaction of the dewar's window to both 80K and vacuum conditions affects the CGH wavefront. Characterization of the window is required in order to subtract window-induced errors in software. An abbreviated procedure for cold testing is as follows:

4. Dewar testing
   - Align and measure both window surfaces of the dewar when at warm, no vacuum conditions.
   - Evacuate the dewar and cool the mirror to ~80 K.
   - Once the cooling rate drops to < 0.1 K per 15 min interval, initiate a 60-minute soaking process.
   - Take three cold vacuum shots of both the dewar window surfaces as well as the test mirror.

- Close the camera shutter between the mirror and window and initiate a second soaking process.*
- Once temperature stability is reached, open the shutter and retake measurements.
- Allow the mirror to warm to ~293K. Remeasure the mirror and window.

## 4. RESULTS

### 4.1. Microroughness

The results of micro-roughness testing with the Phase Shift MicroXAM are listed in Table 2a. Every mirror, with the exception of M4, has been characterized as being slightly over the 10 nm specification. The impact of this component level problem on system level performance is presented by Connelly, et al.[4] Contributing factors to the mirrors' microroughness are the grain structure of the aluminum and the groove structure from the diamond turning process, which is worsened by the inclusions in the aluminum 6061.[3] The grain structure causes a hazy or foggy surface after diamond turning, with a strongly preferred orientation. The aluminum stock contains additional impurities that tend to catch on the diamond tool and cause "snowball" effects across the surface of the mirror. Such inclusion marks are visible in Figure 4a. The dominant feature of this surface profile is the ~30 micron tool period. In our experience, this groove structure is dependent on the degree of impurities in the aluminum being machined.

| Mirror | Average RMS (nm) | 1σ spread in RMS across aperture (nm) |
|---|---|---|
| M1 baseline | 11.0 | 1.7 |
| M1 spare | 17.5 | 3.3 |
| M2 baseline | TBD | TBD |
| M2 spare | 11.9 | 2.6 |
| M3 baseline | 10.5 | 0.5 |
| M3 spare | 10.4 | 1.4 |
| M4 baseline | 8.7 | 0.6 |
| M4 spare | 10 | 0.4 |
| F1 baseline | 11.8 | 5 |
| F1 spare | 9.4 | 2.8 |
| F2 baseline | 10 | 2.5 |
| F2 spare | 7.8 | 3.3 |

(a)

| Mirror | Average RMS (nm) | 1σ spread in RMS across aperture (nm) |
|---|---|---|
| F1 baseline | 1.3 | 1 |
| F1 spare | 1.6 | 1.2 |
| F2 baseline | 1.5 | 0.5 |
| F2 spare | 1 | 0.3 |

(b)

Table 2. (a) Microroughness RMS results in nm. (b) Results for super-polished fold mirrors.

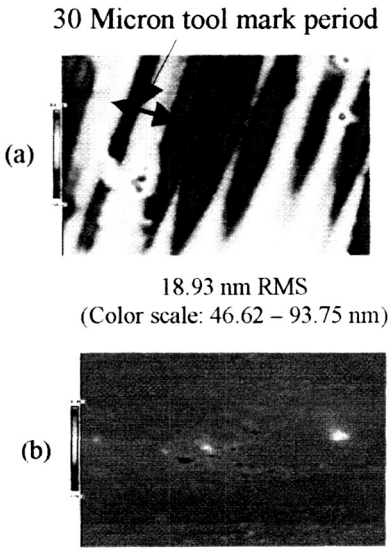


Fig. 4. (a) Surface map of unpolished M1 mirror. b) Surface map of polished F1 mirror.

The much smoother flat mirror surface pictured in Figure 4b is a result of polishing via super-polishing technique .[7] The results are listed in Table 2b. The super-polishing method is only applicable to our flat mirrors, as the process would degrade the figure of the fast, off-axis aspheres.

* In order to minimize the influence of the window's thermal flux on the mirror, a camera shutter is closed between the mirror and window. Realigning the mirror during a 'shutter-test' is troublesome and will be omitted in the future.

### 4.2. Mid-frequency

Results from testing fold mirrors on the Bauer Model 200 Profilometer are show in Figure 5a and Table 3, where the X direction indicates scans that run parallel to the SPDT tool marks and the Z direction indicates scans that run perpendicular to this groove structure. Note that each scan was 20mm long and that the Y scale (in Angstroms) differs between the two plots. Data from the powered mirrors is unavailable due to complications with scanning rougher, aspheric surfaces. While no official instrument requirement exists for mid-frequency errors, we are anticipating RMS values < 100 Å after post-polishing. Mid-frequency error is also detected in figure measurements. An example is pictured in Figure 5 b and c.

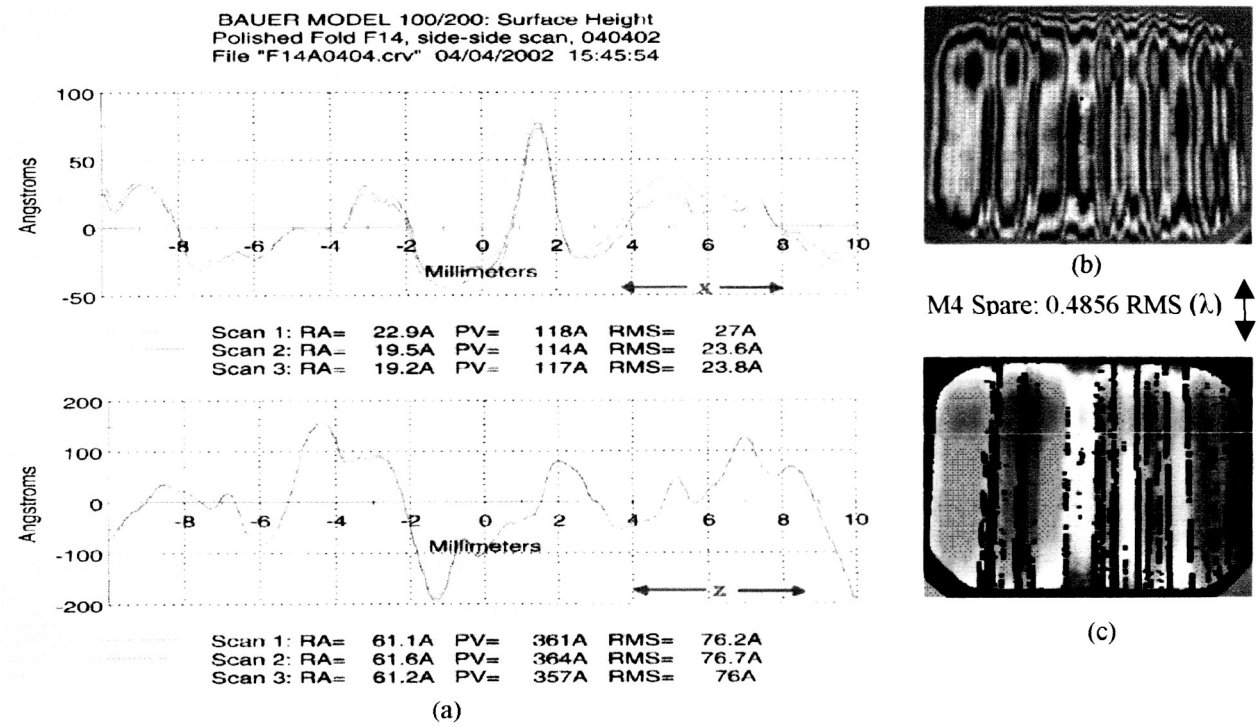


Fig. 5. (a) Orthogonal Bauer scans on flight F1 mirror. (b-c) Example of highly disruptive mid-frequency dominance in a M4 figure measurement.

| Mirror | RMS (X) | RMS (Z) | Spread in RMS |
|---|---|---|---|
| F1 baseline | 24.8 | 76.3 | ~1.56 and 0.29 |
| F1 spare | 60.36666667 | 122.6666667 | ~0.61 and 4.99 |
| F2 baseline | 57.16666667 | 132.3333333 | ~4.44 and 0.47 |
| F2 spare | 67.7 | 122.3333333 | ~0.71 and 0.47 |

Table 3. RMS results of Bauer scans on both fold mirrors.

### 4.3. Figure Error (warm)

Results of null testing each mirror are listed in Table 4. The M3 mirrors met their full aperture specifications. Mirrors M1, M2, and M4 are worse than specification over the full aperture. None of the powered mirrors meet their sub-aperture figure requirements. However, the tolerance analysis assumes figure error that is equally dominated by astigmatism and spherical aberration and the measured surfaces are better than that conservative assumption. The measured figure error of each mirror is typically composed of a combination of lower order terms (e.g., astigmatism, spherical aberration, and coma) and mid-frequency errors (e.g., tool marks). While the measured RMS values apparently do not meet their specifications, the less deleterious contribution of lower order terms allows the mirrors to meet instrument image requirements when these data are included in an as-built instrument model. The two wavefront maps shown in Figure 6 provide a comparison between figure error dominated by lower order terms and figure error dominated by higher order terms. When the mirrors tend to be less rough on larger spatial periods, smaller spatial period, mid-frequency errors tend to dominate the RMS. Thus, the diamond machining grooves are more apparent in the measurement of the baseline M3. The spare M1's blurred surface map is dominated by lower-order terms confirmed by its higher RMS value.

| Mirror | Full Ap. RMS (λ) | | Sub-Aperture RMS (λ) | | |
|---|---|---|---|---|---|
| | Spec. | Data | Spec. | Data | Ap. Dia. (mm) |
| M1 baseline | < 0.1 | 0.213 | < 0.047 λ | 0.086 | 50 |
| M1 spare | < 0.1 | 0.203 | < 0.047 λ | 0.097 | 50 |
| M2 baseline | < 0.1 | 0.689 | < 0.053 λ | 0.341 | 160 |
| M2 spare | < 0.1 | 0.632 | < 0.053 λ | 0.330 | 160 |
| M3 baseline | < 0.1 | 0.080 | < 0.039 λ | 0.062 | 40 |
| M3 spare | < 0.1 | 0.091 | < 0.039 λ | 0.072 | 40 |
| M4 baseline | < 0.1 | 0.224 | < 0.043 λ | 0.135 | 40 |
| M4 spare | < 0.1 | 0.450 | < 0.043 λ | 0.263 | 40 |
| F1 baseline | < 0.1 | 0.084 | < 0.053 λ | 0.042 | 60 |
| F1 spare | < 0.1 | 0.097 | < 0.053 λ | 0.047 | 60 |
| F2 baseline | < 0.1 | 0.067 | < 0.048 λ | 0.037 | 40 |
| F2 spare | < 0.1 | 0.117 | < 0.048 λ | 0.045 | 40 |

Table 4. RMS figure error values in waves at λ=632.8 nm.

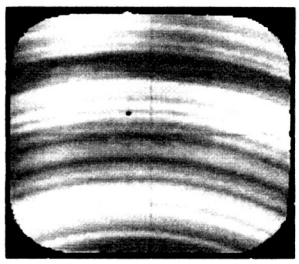

(a)

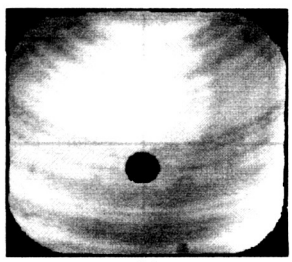

(b)

Figure 6. a) 0.0797 λ RMS figure error of M3. b) 0.2026 λ RMS

A concern with CGH null testing is ensuring that the position of the mirror under test is indeed at global best-alignment position. In order to validate system alignment, we adjusted the mirrors out of alignment in rotation by increments of three arcmin and recorded the wavefront interferograms. The test results from mirrors M3 and M4 are illustrated in Figure 7. By adjusting the mirror in tip ($R_X$) and tilt ($R_Y$), compensating decenters varied linearly and ranged approximately +/-1.9mm. The data are compared to results from a ray trace model to ensure that our best alignment positions were not local minima.

Mirror fiducial characterization for 'as-built' alignment positions proved to be problematic. We attempted to map the translations and rotations of the as-built mirror alignment fiducials to the CGH fiducials, but the data were inconsistent between trials with scatter as large as several arcmin in rotations and 0.25—0.5 mm in translations. Each mirror's 'as-built' best alignment position remains essentially uncharacterized relative to the CGH alignment fiducials. However, the

mirror and CGH alignment fiducials were very useful for rough alignment of the mirror to the CGH. This result was not expected and is an important "lesson learned."

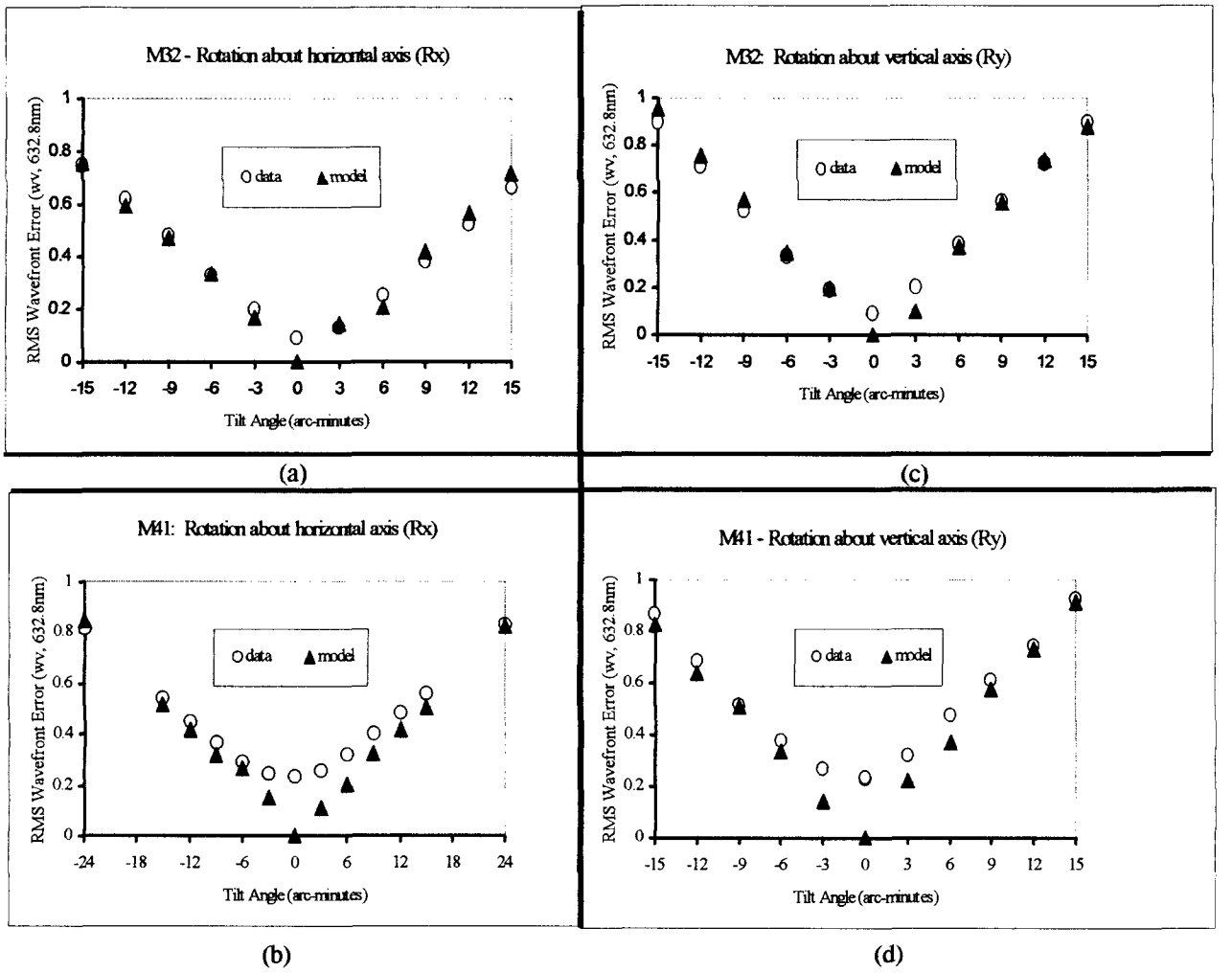


Figure 7. a)-b) RMS wavefront error as a function of tip ($R_X$) misalignment angle for mirrors M3 and M4. c)-d) RMS wavefront error as a function of tilt ($R_Y$) misalignment angle for mirrors M3 and M4.

### 4.4 Figure Error (cold)

Results from testing mirror M3 at 80K are displayed in Figures 8 and 9. In both examples, effects from the dewar's window and mirror prescription change have been subtracted using commercial software (Section 5). Figure 8 shows that M3's figure degrades to worse than the 0.1 λ RMS specification. The change in figure error is expected to be about 0.05 λ RMS for a stress-relieved mirror. [5] Subtracting the warm figure error data from the cold array (entry-wise) for three thermal cycles produced the data depicted in Figure 9. Cold testing completed on a component level (i.e., the flat mirrors and M3) indicates that the mirrors will not deform radically at operating temperature.

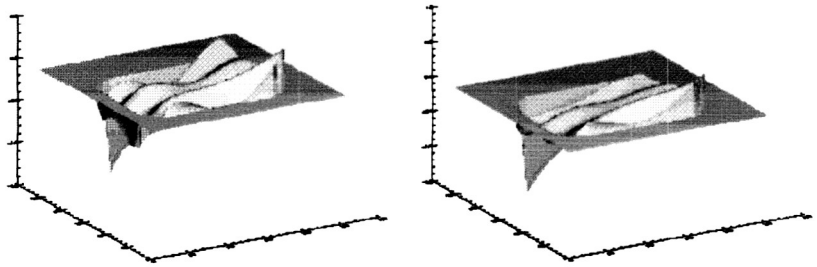


Figure 8. (a) M3 baseline at 293K (0.094 λ RMS). (b) M3 baseline at 80K (0.124 λ RMS).

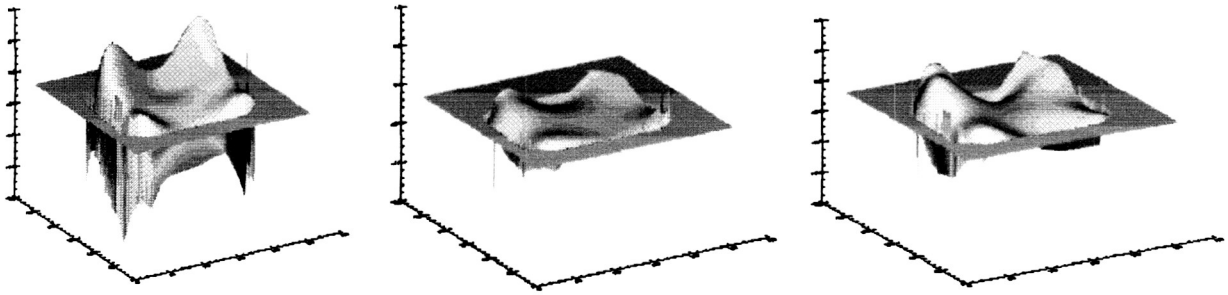


Figure 9. Figure error change for three cold cycles (80K to 293K). a) First cycle: 0.088 λ RMS b) Second cycle: 0.046 λ RMS c) Third cycle: 0.048 λ RMS

## 5. COLD TEST DATA REDUCTION

Reduction of the data from the mirror cold tests remains a "work in progress" as of this writing, but useful results have been obtained from the method developed thus far. The desired result of the data reduction algorithm for a given test trial was to obtain the mirror's figure error at 80K. Three sources of measured figure error arise in the cold test which are not present in the room temperature test. The first is the expected mirror figure change due to the theoretical 0.398% shrinking of the aluminum 6061 mirror's dimensions between 293K and 80K.[5] The second is the contribution of the test dewar window to system wavefront error, which deforms into a meniscus shape under vacuum, followed by a slight return toward its undistorted form when the dewar is cooled to ~80 K. The third is the unknown change in figure due to stresses in the aluminum mirror. Removing the contribution of the first two to detect the third component is the goal.

ZEMAX™ is chosen to process the data because the Zernike surface choices in the program provide a convenient means to place interferometrically measured figure error onto a modeled surface.* For each test trial, the two dewar window surfaces are measured using a reference flat on the interferometer. The window outer surface figure is obtained directly from the measured wavefront by using the phase measuring software's Zernike polynomial fitting capability. A 36-term

* Focus Software, Inc., P.O. Box 18228, Tucson, Arizona 85731 USA

polynomial sum, is fit to the measured wavefront and scaled by 0.5 to obtain the actual surface figure. The coefficient values are then placed on the window outer surface in a model of the interferometric test of the window inner surface.

Obtaining the figure of the window inner surface is trickier because the wavefront reflected from that surface passed through the outer surface and the window substrate twice before being measured (at 80K, the substrate may develop an index or thickness gradient due to a radial temperature gradient)[5,12]. This is accomplished by first entering the Zernike coefficients (in units of waves, scaled to unity) fitted from the wavefront measured off the inner surface, to the merit function of the window test model. The window inner surface is then set as a Zernike Fringe Sag surface, with the coefficients set as variables. The values of the coefficients are then adjusted (the model optimized) until the system performance targets are reached (merit function minimized). This algorithm yields the window's actual figure for each test trial.

With the window's figure in hand, it is straightforward to obtain the mirror's cold figure error. In a model of the mirror cold test, the mirror's theoretical cold figure is placed on the mirror's surface, and the window's surface figures, obtained by the method detailed above, are placed on the window surfaces. The mirror's measured wavefront, which includes the error contributed by both the window and the expected shrinkage of the mirror, is fitted by a 36-term Zernike polynomial sum. The coefficients from this sum (units of waves, scaled by –1) are then placed on the mirror's surface in the model. When rays are traced through this system, the influences on the wavefront of the expected mirror figure change and dewar window are effectively removed, yielding a modeled wavefront that closely approximates the mirror's cold figure error alone. This algorithm was tested by comparing measurements of M3's figure with and without the dewar window in the optical path. With the window present, the system is tested both at ambient pressure and under vacuum. For both cases, the modeled wavefront with the window influence removed closely matched the measured wavefront without the window in terms of qualitative appearance and RMS figure error amplitude. For one M3 mirror with no window in the optical path, the measured RMS figure error (with polynomial fit residuals removed) is 0.081 $\lambda$. For the window, ambient pressure case, the modeled RMS is 0.077 $\lambda$, and for the vacuum case the RMS is 0.078 $\lambda$.

## 6. TOLERANCE ANALYSIS

For each mirror tested, the CGH vendor prepared a detailed tolerance analysis for the test.[13] The largest potential error sources (not including alignment) were due to interferometer and CGH substrate contributions to the wavefront error. The budgeted tolerance for the interferometer was 0.020 $\lambda$ for each test, and ranged from 0.006 to 0.016 $\lambda$ for the CGH transmitted wavefront distortion (TWD). The CGH TWD was measured by the vendor and provided the stated tolerance. Prior to testing the *IRMOS* mirrors, each interferometer used for testing was checked by testing a reference spherical mirror with RMS wavefront error certified to be < 0.010 waves. For both interferometers, the measured RMS wavefront of the reference mirror fell below 0.015 $\lambda$. After testing several of the *IRMOS* mirrors, it was determined that the contributions from the interferometer and CGH were not significant enough to warrant accounting for their influence during mirror test data reduction.

The 15 cm diameter biconvex lens required for the M1 test provided an additional source of error. The radii of curvature of the lens surfaces were measured by the lens vendor and incorporated into the design of the CGH. Unknown errors in surface figure, thickness, and index contributed 0.046 waves RMS to the error budget and needed to be accounted for. To measure these errors, a CGH test was designed specifically for the lens. This test showed that the lens error, with contributions from the interferometer and the lens CGH removed, was 0.021 waves RMS. This was also considered to be insignificant relative to the RMS figure error of M1, and so was not removed to obtain the M1 results.

## 7. CONCLUSION

Optical testing of the *IRMOS* mirrors show that they essentially meet specifications for figure error. Figure error testing at ~293 K demonstrates that several mirrors do not meet the vendor specification for figure error, yet meet instrument image requirements when included in an as-built instrument model. Cold testing at ~80 K has thus far established that the mirrors will not deform in an unanticipated manner during transition to the operating temperature. Both

microroughness and mid-frequency error measurements illustrate a problematic, periodic groove structure from the diamond machining process. Their effects will be mitigated on the system level by characterization, modeling, stray-light baffling, and data reduction. Problems with characterizing as-built mirror optomechanical alignment fiducials on a component level have provided an important lesson learned.

## ACKNOWLEDGEMENTS

We are indebted to the hard work and dedication of those who contributed to the *IRMOS* project. Specifically, we thank Louis R. Worrell Jr. and the Management Technology team for fabrication and test support, Linette D. Kolos of GSFC for post polishing, Mike P. Barthelmy and Bruno F. Munuz of GSFC for stress relieving the mirror blanks, the mechanical team for design work, as well as Leroy M. Sparr, Shane Wake and Donald H. Sexauer for CGH test support. *IRMOS* greatly acknowledges funding support from the *Next Generation Space Telescope* project at the NASA/Goddard Space Flight Center and the Director's Discretionary Research Fund at both the GSFC and the Space Telescope Science Institute.

## REFERENCES

1. J.W. MacKenty, M.A. Greenhouse, R.F. Green, L.M. Sparr, R.G. Ohl, R.S. Winsor, "IRMOS: An Infrared Multi-Object Spectrometer using a MEMS micro-mirror array", Proc SPIE 4841, 2002.
2. R. S. Winsor, J.W. MacKenty, M. Stiavelli, M. A. Greenhouse, J. E. Mentzall, R. G. Ohl, and R. F. Green, "Optical design for an *Infrared Multi-Object Spectrometer (IRMOS)*," *Proc. SPIE* **4092**, pp. 102-108, 2000.
3. R. G. Ohl, W. Preuss, A. Sohn, S. Conkey, K. Garrard, J. G. Hagopian, J. M. Howard, J. E. Hylan, S. M. Irish, J. E. Mentzell, M. Schroeder, L. M. Sparr, R. S. Winsor, S. W. Zewari, M. A. Greenhouse, and J. W. MacKenty, "Design and fabrication of diamond machined, aspheric mirrors for ground-based, near-IR astronomy," *Proc. SPIE* **4841**, 2002.
4. J. A. Connelly, R. G. Ohl, T. T. Saha, T. Hadjimichael, J. E. Mentzall, R.G. Mink, V. J. Chambers, M. A. Greenhouse, R.S. Winsor, and J. W. MacKenty, "Imaging performance and modeling of the *Infrared Multi-Object Spectrometer* focal reducer," *Proc. SPIE* **4841**, 2002.
5. R. G. Ohl, M. P. Barthelmy, S. W. Zewari, R. W. Toland, J. C. McMann, D. F. Puckett, J. G. Hagopian, J. E. Hylan, J. E. Mentzell, R. G. Mink, L. M. Sparr, M. A. Greenhouse, and J W. MacKenty, "Comparison of stress relief procedures for cryogenic aluminum mirrors," *Proc. SPIE* **4092**, 2002.
6. ZEMAX. *Optical Design Program, User's Guide, Version 9.0*, p. 305, Focus Software Inc., Tuscon, AZ, 2000.
7. J. J. Lyons III and J. J. Zaniewski, "Process for polishing bare aluminum to high optical quality", *NASA Tech Briefs*, **23**, 58--59, 2001.
8. P. Glenn, *Bauer Model 100/200 Windows Software Manual*, 2001.
9. P. Glenn, "Robust, sub-angstrom level mid-spatial frequency profilometry," Proc. *SPIE* **1333**, pp. 175-182, 1990.
10. J. Houston, C. Buccini, and P. O'Neill, "A laser unequal path interferometer for the optical shop," *Appl. Opt.* **6**, pp. 1237--1242, 1967.
11. D. Malacara, Optical Shop Testing, pp. 757--758, John Wiley and Sons, Inc., New York, 1992.
12. A. Ahmad, Ed., *Handbook of Optomechanical Engineering*, p. 57, CRC Press, Boca Raton, 1997.
13. S. M. Arnold, L. C. Maxey, J. Rodgers, and R.C. Yoder, "Figure metrology of deep general aspherics using a conventional interferometer with a CGH null," *Proc SPIE* **2536**, pp. 106--116, 1995.